MAGNETIC ANOMALIES ON IO AND THEIR RELATIONSHIP TO THE SPATIAL DISTRIBUTION OF VOLCANIC CENTERS

A Thesis

by

JOSHUA JAMES KNICELY

Submitted to the Office of Graduate and Professional Studies of
Texas A&M University
in partial fulfillment of the requirements for the degree of

MASTER OF SCIENCE

Chair of Committee,	Mark E. Everett
Committee Members,	David W. Sparks
	Kevin Krisciunas
Head of Department,	Rick Giardino

May 2015

Major Subject: Geophysics

ABSTRACT

Forward modeling of planetary-scale magnetic anomalies due to induced crustal magnetization of Io is developed. My approach involves finite difference modeling of a temporally- and spatially-averaged steady state geotherm superimposed by the thermal evolution of an instantaneously emplaced volcanic pipe. Previous authors have estimated the steady state geotherm of Io. A slight adjustment to their parameters results in a preferred steady state geotherm that is colder at depth. The crustal magnetization is determined based on the calculated distribution of temperature and the ambient Jovian magnetic field. Magnetite is assumed to be the dominant magnetic mineral. Io resides in a time-varying magnetic field produced by Jupiter that is idealized herein as a uniform field of 1835 nT. The thermal data are converted to magnetization of discretized crustal prisms using a temperature-dependent susceptibility. Synthetic flyby data as would be observed by a satellite are generated along certain meridional swaths of Io's surface. The swath locations are selected based on observed locations of volcanic centers, hotspots, and accumulations of ejected volcanic material.

This work produces a 1 D geotherm which remains at approximately the surface temperature to within a few kilometers of the thermal lithosphere/mantle boundary. This solution shows little dependence on porosity due to the depth at which rapid temperature change occurs. These conclusions hold for largely varying mantle temperatures. Silicate volcanic centers cool to temperature of sulfur volcanism rapidly and become indistinguishable within 10,000 years. The magnetic anomaly due to temperature

variation is smaller than detectable in current conditions. If a crustal anomaly is detected by future satellite missions, it would suggest drastically different conditions at Io in the geologically recent past.

ACKNOWLEDGEMENTS

I would like to thank Dr. Everett and Dr. Sparks for the copious amounts of time they have spent helping me reach this point. I would also like to thank family, friends, and strangers that have allowed me to explain my research to them and torture them with other science.

TABLE OF CONTENTS

LIST OF FIGURES

1. INTRODUCTION

Io is the most volcanically active body in the solar system due to tidal heating. The intense heating is produced by a Laplace orbital resonance with Jupiter and the surrounding moons. The volcanic edifices and mountains provide information useful in determining the predominant heating processes, the synchronicity of the moons rotation, and the crustal thickness, but these structures are only surface expressions. Resurfacing rates of 0.1-1 cm/yr obscure most topographic features under a veneer of sulfur within 1 Myr (5, 10). The magnetization of Io's iron-bearing crust, beneath the non-magnetic sulfur layer, encodes information about the fundamental geologic processes operating in its interior. The magnetic anomalies generated by the spatial variations in magnetization, can be mapped by future satellite magnetometer missions. Examination of the magnetic anomaly pattern due to crustal magnetization of Mars, for example, indicates the past presence of a powerful magnetic field and an early stage of plate tectonics as deduced from observed magnetic stripes and apparent transform faults. The magnetic anomaly pattern on Mars contributes to the hypothesis that many of the extant great volcanic edifices on that planet were created by motion of the crust over two fixed hotspots that episodically broke through the surface (6).

In this thesis, I develop a synthetic magnetic anomaly map of Io as it would be seen by a magnetometer aboard a satellite flyby. A magnetic anomaly map displays the magnetic field intensity due to natural remanent magnetism (NRM) of crustal rocks. In this thesis, I limit the consideration of NRM to the thermoremanent magnetism (TRM)

contribution and do not consider any past variation in the direction of the ambient Jovian field. As I assume the field direction and strength of the Jovian field at Io to be constant and uniform, the induced magnetization and TRM will be the same. Typically, induced and remanent magnetization are considered two distinct parts that combine to form the total magnetization ($J_{total} = J_{induced} + J_{remanent}$) (3). In this work, the magnetizing field is assumed constant and uniform. While this is very inaccurate on a short time scale as the field oscillates rapidly, the periodic nature of the oscillation over the course of Io's orbit around Jupiter should, as a bulk material, be equivalent to a single magnetic direction. This means the induced and remanent fields are treated as the same, though the true induced component will vary.

Radially-symmetric thermal modeling in 2-D cylindrical geometry is used to determine the likely thickness of the magnetized crustal layer around a recently-active volcanic center. Using this model of the magnetization of the crust, a standard technique of discretizing the region into prisms and summing the magnetic field of each prism (2) is used to obtain the crustal magnetic anomaly map around a recent volcanic center. The mapping is conducted in meridional swaths so that Cartesian geometry may be used to simplify the analysis. Figure 1 is a conceptual depiction of the volcano, magnetization, and satellite flyby. The magnetic anomaly analysis is performed for different supposed magnetic properties of the prevailing mafic and ultramafic materials comprising Io's crust.

2. BACKGROUND

Io is the most volcanic body in the solar system due to tidal heating caused by the time-varying gravitational forces exerted on Io by Jupiter and its other moons (5, 10, 24, 27). The primary source of these variations are the Galilean moons and Jupiter. Io, Europa, and Ganymede are in a Laplace resonance in which for each orbit Ganymede makes around Jupiter, Europa makes two and Io makes four. The orbital period of Callisto, the outermost of the Galilean moons, is slightly longer than that required for a Laplace resonance. The varying gravity causes tidal deformation of Io as large as 100 meters (5, 27). Typical deformation amplitudes are much smaller and occur over very short time periods of only a few days (5, 27). Viscous dissipation due to millions of kilograms of deforming rock produces prodigious amounts of heat and volcanism (21, 27). Io is thought to be covered by thin veneer of sulfur overlying mafic to ultramafic rock that together comprises a lithosphere 20-50 km thick (8, 10, 13). This estimate of lithospheric thickness is based on the ~6-17 km heights of the mountains on Io and the predominant hypothesis for their formation (5, 33). Surface striations and analyses of mountain topography show that many of Io's mountains are steep-sided tilted blocks undergoing tectonic collapse (5, 21, 23, 33). On a global scale, the volcanic output of Io continually buries the lithosphere in lava and ash, forcing it downward into the interior of the moon. As burial progresses, horizontal compressive stresses increase faster than vertical stresses, as a given volume of lithosphere becomes squeezed into a smaller volume. It is likely that the lithosphere breaks and portions of it tilt to accommodate the compression (5, 21, 23). A lithosphere at least 14 km thick is required to provide

sufficient compressive stress, and, under this mechanism of mountain formation, the lithosphere must be at least as thick as the tallest mountains (21). Reference 21 and 23 report a minimum depth estimate to the thermal lithosphere of 12 km. The foregoing estimates are lower limits of lithospheric thickness. Upper limits are poorly constrained and range from 25 to 100 km (21, 23). Along with many *Galileo* era scientists, I adopt a nominal lithospheric thickness value of 30 km (5).

The mountains and paterae share an obvious connection. The locations of volcanic centers and mountains are apparently random at a quick glance. This is in stark contrast to volcanoes and mountains on Earth which typically form as a linear suite. Statistical analysis of their locations has revealed these edifices are not randomly located. Volcanoes are evenly distributed near equatorial latitudes and are more randomly distributed near the poles. Paterae and mountains often occur in close proximity, though the volcanoes are more numerous (5, 8, 12, 14, 33). According to reference 14, there are 3 dominant hypotheses to explain their relationship; mantle upwelling causes the fracturing and tilting of the crust to form mountains and magma is able to travel along the newly formed faults; mantle downwelling causes excess compressive stress and creates mountains and faults by which magma can travel; and disruption of a volcanic center will cause local increase in the geothermal gradient, the host rock undergoes thermal expansion creating excess stress and mountains form. All of these predict a particular distribution of volcanism and mountains. Current distributions are based solely on surface expression (8, 14).

Both sulfur based and silicate volcanism occur on Io. During the *Voyager* pass of Jupiter, temperatures only up to 700 K, the cut-off for sulfur volcanism, were measurable (5, 20). For many years, there was debate on the existence of silicate volcanism of any form on Io. More exact temperature measurements were able to clearly show that silicate volcanism also occurs on the surface of Io (5, 20).Whether sulfur volcanism can occur independently or is always linked to silicate volcanism is uncertain. The silicate volcanism of Io works similarly to that of terrestrial calderas. A dike of magma rises towards the surface until it reaches a point of neutral buoyancy. Due to the porosity of the crust and interstitial sulfur reducing bulk density, the point of neutral buoyancy is only a few kilometers from the base of the lithosphere (5, 17). Because of this, the rising dike should stall until the magma density drops below that of the host rock by magmatic differentiation or the introduction of volatiles. A possible mechanism to introduce volatiles is sulfur and sulfur dioxide aquifers. At high pressures and relatively low temperatures of 400 K and 200 K, both sulfur and sulfur dioxide exist as liquids. The compressive stress regime of the crust creates numerous fracture pathways by which this liquid can travel. The depth at which these aquifers form is typically lower than the neutral buoyancy point of the magma. The magma reaches these aquifers and incorporates the volatile sulfur and sulfur dioxide. This greatly reduces the magma density and enables it to nearly reach the surface (12, 17). Very close to the surface is a layer of nearly pure sulfur and sulfur dioxide frost above which the magma cannot rise due to buoyancy alone. Laterally compressive stresses in the crust can provide the necessary energy to force lava onto the surface. The intense heat of the lava and magma

melts and vaporizes surrounding volatiles, forming a caldera-like structure called a patera (5, 12, 17, 20, 21). The distribution of paterae has been used as a proxy for heat flux to model and better understand the tidal dissipation process in Io (8).

Io has numerous volcanic centers that are commonly held to be mafic to ultramafic in composition. This supposition owes to the unusually high temperature readings acquired by satellite-borne sensors (4, 8, 10, 12, 18, 19, 20, 21). Eruption temperatures range as high as 2600 K, which is incredibly difficult to explain by any method, but have very large error bars (11, 19). The 1997 Pillan eruption, which has the best constrained temperature estimates, requires a minimum eruptive temperature of ~1610 K, the highest recorded minimum temperature (11). Approximately 100 K of heating is estimated to occur due to viscous dissipation within the magma during ascent (11). This suggests a magma temperature in the upper mantle of ~1500 K or greater, making terrestrial (tholeiitic) basalt, with a liquidus of ~1430 K, an unlikely analogue of the volcanic material on Io (11, 34). The number of volcanic observations that allow for such high temperatures is relatively sparse and may represent only a subset of the silicate volcanism occurring on Io.

Spectral analysis of the mineralogy of dark spots on Io suggests the silicate magmatism to be of a single type. Laboratory-based spectral analysis of orthopyroxene, a Mg-rich silicate mineral, provides the best fit to the observed spectra from *Galileo* for the dark units that coincide with hotspots. This observation suggests the presence of mafic to ultramafic materials (12, 20, 33). Flow rheology reflects extremely low viscosity lavas, indicative of ultramafic lavas (31). Typically, spectral analysis of rock is

very simple and allows for very exact matching of mineralogy. Problematically, the Near Infrared Mapping Spectrometer (NIMS), originally meant to be a hyperspectral system with hundreds of spectral bands, suffered damage and was reduced to only 13 spectral bands by the time *Galileo* began close observations of Io (20), introducing uncertainty into darkspot composition. Commondale komatiite has previously been proposed as a likely analogue due to its high MgO content and its inferred high liquidus temperature of ~1880 K (34). However, Lunar Mare basalts have a liquidus of ~1710 K and may also represent an accurate analogue (34).

The magnetic field that magnetizes Io's crust originates in the dynamo of nearby Jupiter. The Jovian magnetosphere is many times larger and more powerful than Earth's and extends beyond Io's orbit. The orbit of Io remains inside this dipolar external magnetic field. The average magnetic field along Io's orbit is 1835 nT (32). The movement of Io through Jupiter's magnetosphere exposes it to a time-varying magnetic field. This fact has been used to add credence to the magma ocean hypothesis. Reference 12 proposed a global mushy magma ocean underneath the lithosphere with as much as 50% melt. Such an ocean would keep the bottom of the lithosphere at a near constant temperature, and continuous burial would cause the bottom to be quickly be melted and then remixed (20, 21). In a liquid state, the electrical conductivity of ultramafic and mafic materials increases orders of magnitude and creates a response in a time-varying magnetic field (3). This causes a low frequency deviation of the field near Io from background value by several hundred nT (13). Reference 13 explored this via EM sounding of magnetometer data from *Galileo* passes I24 and I27, with closest passes of

615 and 201 km, respectively. They estimate an approximately 50 km thick mushy magma ocean of ~20% melt.

In addition to these external and internal contributions to the Io magnetic field is that of the plasma torus linking Io and Jupiter (18). The magnetic effect of the plasma torus is regarded herein as an extraneous secondary field, similar to the auroral-latitude ionospheric field on Earth. Such additional signals can be removed from flyby or other satellite-acquired magnetic field data to obtain a reduced dataset that reflects primarily the source of interest, which, in this case, is the field due to crustal magnetization, and has been done with the *Messenger* flyby data to exclude the effects of plasma and the solar winds near Mercury to produce spherical harmonic functions that describe the internal magnetic field generated by the permanent magnetization of that planet (1, 16).

Galileo obtained several magnetometer data sets while passing within several thousand km of Io. Two are high-quality data. These are I24 and I27, with closest approaches of 615 and 201 km. These can be seen in reference 15. At closest approach, the magnitude of the magnetic signal is smoothly varying. The vectorial components of I24 show a relatively smoothly varying signal near Io which becomes polluted with high-frequency and high-amplitude noise as *Galileo* passed the moon. The components of I27 became noisy, with perturbations of several tens of nT as *Galileo* approached Io. Reference 15 attributed these perturbations to plasma currents. The *Io Volcano Observer* is scheduled to launch in 2015 or 2016 with two fluxgate magnetometers on board (22). Plans for this satellite involve passing within 100 km of Io directly through a volcanic plume. The magnetometers are designed to achieve an accuracy of 0.25 nT for a base

reading of 50 nT and a 0.12 nT sensitivity. Near Io (within 20 Io radii), readings will be acquired thirty times per second.

The magnitude of the bulk magnetization of Io's crust depends on the ambient inducing field, but also on the crystal domain structure of crustal rocks and the proportion of magnetic minerals contained in the rock. Common magnetic minerals include magnetite and hematite. Induced magnetization is often strongly correlated to magnetite content and will be the only magnetic mineral considered in this thesis. The thermoremanent magnetization of magnetite becomes zero at the Curie temperature, the temperature at which thermal perturbations randomize the dipoles of a material. For magnetite, this temperature is 858 K. Pyrrhotite is a less common magnetic mineral on Earth composed of iron and sulfur, but may be more common on Io, and, along with hematite, should be considered in future work. The abundance of magnetic minerals is usually quite low in unaltered mafic rocks (only a few percent). The type of primary minerals that form from an igneous melt depends on the composition of the melt and oxygen fugacity. Magnetic minerals can also form by exsolution at intermediate temperatures and can be affected by deuteric oxidation (3).

3. PREVIOUS WORK ON THE STEADY STATE GEOTHERM OF IO

A steady state geotherm for Io has been determined analytically by reference 26, who derived their solution for locations away from volcanic centers. The thermal diffusivity, κ, density, ρ, specific heat, c_p, and the heating rate per unit solid, H, are held constant. The governing equation for temperature, T, is

$$\frac{\partial T}{\partial t} = \nabla(\kappa \nabla T) + \frac{H}{\rho c_p} - v\nabla T \qquad \kappa = \frac{k}{\rho c_p} \tag{1a}$$

Reference 26 solve a one-dimensional version of equation (1a) for $T(z)$ in the simplified case in which the radiative decay term, $\frac{H}{\rho c_p}$, is neglected. The advection of the crust is uniformly downward at velocity v. This value is the global average rate at which Io is resurfaced and previously emplaced crust is buried and forced downward. The model assumes the lithospheric thickness reaches a maximum value, d, where the temperature is fixed at a magma temperature, T_m. The steady-state heat equation is

$$0 = \nabla(\kappa \nabla T) - v\nabla T \tag{1b}$$

The solution to equation (1b), subject to fixed temperatures at the thermal lithosphere boundary and the surface, respectively T_m and T_s, is given by

$$T(z) = \frac{(T_m - T_s)(\exp\left(\frac{z}{l}\right) - 1)}{\exp\left(\frac{d}{l}\right) - 1} + T_s, \tag{2}$$

where $T(z)$ is the temperature at depth z, $l = \kappa/v$ is the constant thermal diffusivity divided by the constant advective velocity, and d is the maximum thickness of the lithosphere. The velocity is calculated to be 1.12 cm/yr using equation (3), below, and thermal parameter values from reference 17. In reference 17, F_a is the total volcanic heat flux emitted by the planet, ρ_m is the density of the magma, ΔH is the latent heat of crystallization, and C_{pa} is the average specific heat.

$$F_a = v\,\rho_m\left[\Delta H + C_{pa}(T_m - T_s)\right] \quad (3)$$

Reference 17 extend the work of reference 26 by use of a finite difference model to include the temperature and porosity dependence of thermal diffusivity. In both models, the lithosphere of Io remains cold (close to the surface temperature) to the base of the crust/thermal lithosphere (17). A total heat flow estimate for Io based on thermal emission measurements is approximately the same as values of heat flow from hot spots (21). This indicates that hot spots and volcanic activity account for most of Io's heat flow (21).

Reference 17 use the temperature-dependent diffusivity developed in another work, namely

$$\kappa(T) = \begin{cases} 441.48 \times 10^{-6} \times T^{-1} - 4.825 \times 10^{-8}, T < 832.25 \\ 5.696 \times 10^{-7} - 1.0506 \times 10^{-10} \times T, T > 832.25 \end{cases} \quad \text{m}^2/\text{s} \quad (4)$$

This relationship was originally derived for felsic and intermediate materials on Earth. Reference 17 multiply $\kappa(T)$ in equation (4) by a factor so that the thermal diffusivity matches measured values of mafic and ultramafic materials at their liquidus temperatures. Thermal diffusivity is correlated to both silica and quartz content, but shows a stronger correlation to the latter. The silica content can be used as a first order approximation of the quartz content, which is pure silica (SiO_2) (30). Silica content varies with mineralogy. Generally, ultramafic rocks have the lowest silica content and felsic rocks have the highest silica (and quartz) content. Exceptions to this exist, but are uncommon. The greater the quartz content, the greater the thermal diffusivity at low temperatures. As the silicate materials of Io are expected to be mafic to ultramafic in composition, quartz (and silica) content should be significantly lower than that of felsic and intermediate materials. For this reason, I use instead the set of equations for thermal diffusivities of lunar materials determined by reference 7. Their equations were determined for temperatures ranging from 85-850 K for three different Lunar Mare basalt samples. The particular equations I use apply to samples with moderate and high porosity (5.5% and 11.0%) in vacuum. The value obtained at 850 K is used for all higher temperatures. The expressions are

$$\kappa(T) = \begin{cases} 3.05 \times 10^{-9} + \frac{0.4 \times 10^{-6}}{T} + 1.26 \times 10^{-18} \times T^3, \ n = 5.5\% \\ 1.3 \times 10^{-9} + \frac{0.27 \times 10^{-6}}{T} + 4.38 \times 10^{-18} \times T^3, \ n = 11.0\% \end{cases} \text{ m}^2/\text{s} \quad (5)$$

Additionally, the thermal diffusivity is modified by the porosity approximation outlined by reference 17. This approximation assumes a maximum porosity (the surface value) that decreases with depth due to overburden pressure. The porosity is a function of simple first-order gravity and pressure considerations. The difference between the reference 17 and reference 7 thermal diffusivities is within an order of magnitude ($\sim 5 \times 10^{-7}$ m^2/s), but even this small difference causes significant changes to the calculated steady state geotherm. The difference between the original reference 17 and porosity-modified reference 7 thermal diffusivities is displayed in Figure 2. Modeling by reference 17furthermore shows that radioactive decay results in negligible heating so that it is safely ignored herein.

4. METHODS AND RESULTS

This problem involves two decoupled parts; a thermal portion and a magnetics portion. In the thermal portion, the steady state geotherm of Io is determined by finite difference modeling. The steady state geotherm is then used as the initial temperature distribution upon which the transient thermal effects of a radially symmetric, instantaneously emplaced, volcanic pipe are computed. The transient geotherm is also calculated with a finite difference technique. In the magnetics portion of the work, the temperature values from the thermal calculations are converted, using a temperature-dependent susceptibility formula, into a magnetization for each one of a grid of 2-D discretized crustal prisms. This is done for ten "epochs" during the thermal evolution of the volcanic center to observe changes in the magnetic anomaly through time. The magnetic anomaly, as it would be measured by a satellite magnetometer in meridonal orbit, is then calculated from the summed magnetic effect of the prisms. This procedure is performed for the following sets of parameters; surface porosity equal to 0.1, 0.3, and 0.5; crustal thicknesses of 20, 30, 50, and 90 km; satellite altitudes of 0.001, 1, 10, 100, and 1000 km; volcanic pipe radii of 80 and 160 m. The altitudes of 1 m, 1 km, and 10 km are unreasonable values for satellite flybys, but are useful as a check to ensure proper execution of modeling.

4.1 Thermal Model of Io Crust

The initial step of the thermal modeling is to determine the 1-D steady-state geotherm of Io. The boundary conditions are constant temperatures of $T_S = 90$ K and $T_M = 1500$ K at the surface and base of the thermal lithosphere, respectively. The

numerical algorithm is a flux-conservative, iterative Gauss-Seidel scheme using centered differencing on the diffusion term ($\nabla(\kappa\,\nabla T)$) and upwind-differencing on the advective term ($v\,\nabla T$). This type of numerical scheme is designed to rapidly converge to steady-state. Equation 6b, below, illustrates the flux-conservative approximation and is used in the 1-D equation 6a. In this, $F_{i+\frac{1}{2}}$ is the diffusive flux passing between two nodes.

$$0 = \frac{\partial}{\partial z}(\kappa \frac{\partial T}{\partial z}) - v\frac{\partial T}{\partial z} \approx -\frac{F_{i+\frac{1}{2}} - F_{i-\frac{1}{2}}}{\Delta z} - v\ \frac{(T_i - T_{i-1})}{\Delta z} \tag{6a}$$

$$F_{i+\frac{1}{2}} = \kappa_{i+\frac{1}{2}} \frac{\partial T}{\partial z}\Big|_{i+\frac{1}{2}} = \frac{\kappa_{i+1}+\kappa_i}{2} \times \frac{T_{i+1}-T_i}{\Delta z} \tag{6b}$$

With constant thermal diffusivity, the numerical solution and the equivalent analytical solution are very similar, as shown in Figure 3. There is a slight deviation at intermediate depths where the change in the geotherm is large.

In the region around a volcanic center, transient thermal effects are expected following emplacement of a volcanic pipe. Accordingly, in such regions I solve the 2-D time-dependent diffusion equation (7), below, assuming radial symmetry.

$$\frac{\partial T}{\partial t} = \frac{1}{r}\frac{\partial}{\partial r}\left(\kappa \frac{\partial T}{\partial r}\right) + \frac{\partial}{\partial z}\left(\kappa \frac{\partial T}{\partial z}\right) - v\frac{\partial T}{\partial z} \tag{7}$$

I apply the steady state geotherm calculated above as the initial temperature distribution, and set $T_M = 1500$ K for the temperature of the instantaneously emplaced

volcanic pipe. I use the same boundary conditions as the 1D case for the surface and bottom of the modeling domain ($T_S = 90$ K and $T_M = 1500$ K, respectively). Zero-flux (i.e. symmetric) boundary conditions are applied at the center of the pipe (r=0),

$$\frac{\partial T}{\partial r}(r = 0 \; or \; r = r_{max}) = 0 \tag{8}$$

and at the distant vertical boundary of the modeling domain. The maximum radial extent is 25 times the radius of the volcanic pipe (i. e. 4 km for the largest pipe radius). I chose this relatively small value to avoid excessively long run times during the finite differencing. The value was determined empirically such that the outer radial boundary is outside of the range of the temperature change induced by the pipe.

A wide range of possible pipe radii are explored. These are 5, 10, 20, 40, 80, 160, 320, and 640 m. The smallest pipes in this range will produces only a tiny signal, while the largest are likely to be at or beyond the largest possible pipe that could go through the entire crust. The 2-D thermal calculation is time-stepped until the upper 80% of the pipe has cooled to half the Curie temperature of magnetite (429 K). The thermal state of the volcanic pipe at ten evenly distributed times throughout the evolution is used in the magnetic modeling of the lithosphere.

4.2 Thermal Results

Figure 4 shows the results of the 1-D steady-state thermal modeling. Displayed are the analytical solution for a thermal diffusivity of 4×10^{-7} m^2/s and the numerical solutions for surface porosities of 0.1, 0.3, and 0.5 and for crustal thicknesses of 20, 30,

50, and 90 km. Insets highlight regions of rapid temperature change. In all models, the crust remains cold (approximately the surface temperature) down to about 5- 10 km from the thermal lithosphere boundary. The numerical solutions converge to each other as the crustal thickness increases. The increase of crustal thickness forces the region of temperature variation deeper into the crust, where overlying rock reduces porosity to similar and very small levels. The numerical solutions also become more similar to the analytical solution as the crustal thickness increases, deviating only in the regions of rapid temperature change.

It is important to keep in mind that the temperature used for the thermal lithosphere boundary, $T_m = 1500$ K, represents a lower limit and the actual temperature may be significantly higher. Figure 5 shows the 1-D geotherm for a crustal thickness of 30 km and surface porosity of 0.3 for the analytical and reference 17solutions, and for my geotherms at a thermal lithosphere boundary temperature of 1700, 2000, and 2300 K. Even with these much higher, but plausible, temperatures, the 1-D geotherm is colder than that predicted by reference 17. Again, these colder temperatures occur due to the lower thermal diffusivity of quartz deficient materials at low temperatures.

Figure 6 shows the 2-D thermal evolution in a cross-section of a volcanic pipe of radius 160 m, with surface porosity of 0.5, and crustal thickness of 30 km. The four times shown correspond to initial emplacement, at one third and two thirds of the way to the stopping criterion, and at the stopping criterion. For this pipe, it takes approximately 6,700 years to reach the stopping criterion. Thermal energy diffuses through the crust via conduction. Pores are empty space through which this energy is unable to propagate.

Therefore, an increase in porosity results in a decrease in thermal diffusivity. Because lateral cooling at the surface is slower than at depth, there is a local temperature maximum, or a "bubble" of warm material, near the top of the volcanic. The bubble is carried downward by burial as it slowly cools.

4.3 Magnetic Model

The observed crustal magnetization is dependent on three factors: the strength and direction of the inducing magnetic field; the magnetic susceptibility of the crust; and the satellite flight path. The inducing field is that of Jupiter, with a mean strength of ~1835 nT at the orbit of Io (13). The magnetic effect of the plasma torus can be removed by a similar technique to that used for the *Messenger* data and consequently it can be ignored (1, 16). The periodic time-varying induction response due to movement of Io within the asymmetric magnetic field is also ignored as it does not affect the long-term bulk magnetization of the crust and moreover, it too can be isolated from the crustal magnetization field. Therefore, I assume the field of Jupiter to be uniform in amplitude and constant in direction with respect to Io's crust. I assume the magnetized crust has no previous remanence and is magnetized in the direction of the ambient magnetic field. The crustal magnetization is also presumed to be proportional to the strength of the inducing field.

An important task is to estimate the crustal magnetic susceptibility. I consider magnetite to be the most important magnetic mineral as its susceptibility is typically much higher than that of other magnetic minerals (5). Future work should examine the possible effects of other magnetic minerals such as pyrrhotite, which may be common in

the sulfur rich crust, and hematite, the multi-domain form of which is nearly as magnetic as magnetite. Magnetite grains can be single domain (SD), pseudo-single domain (PSD), or multi-domain (MD). These domain types are related to the grain size; SD are 0.05-1 μm, PSD are 1-20 μm, and MD are greater than 20 μm(5). Each of these domains has characteristic magnetic properties (3, 5). The more rapidly the magma cools, the smaller the crystal grain size. I will consider only SD magnetite for this paper as most of the crustal material is expected to cool very rapidly (11). Also, the TRM of SD grains is, in general, stronger than that of PSD or MD grains (5). Future work should consider the possible effect of PSD and MD magnetite that may develop near and within the volcanic pipe where cooling rates should be slower, thereby allowing time for the growth of larger grains. The mass fraction of magnetite is a complicated function of the parent magma composition, ambient conditions at formation, and geological history.

An initial step is to look for terrestrial analogues of the rocks that are expected on Io. However, all accessible terrestrial ultramafic samples of likely analogues have been metamorphosed to some extent, often resulting in large changes to their magnetic properties. Commondale komatiites, which are favored as a possible ultramafic analogue to the silicate materials on Io, have undergone a measure of metamorphism. Exposure to water, for example, results in serpentization, which converts the dominant igneous mineral olivine into the hydrated silicate minerals. The serpentinization reaction also produces large amounts of magnetite, a mineral that is several orders of magnitude more magnetic than unaltered minerals. Water is not expected at Io however, making it highly unlikely for serpentinization to occur. Unaltered ultramafic materials, such as

periodotite, generally have lower magnetite content than mafic rocks, such as basalt (5). Given the crustal composition from reference 11, experimental petrology and normative mineralogy can predict the unaltered mineralogy. I consider the quantitative determination of magnetite content to be beyond the scope of my work and will present the magnetic signal produced by a crust entirely composed of magnetite. The signal can then be scaled for any magnetite content (e.g., if 1% magnetite is presumed, then the signal would be 1% of that calculated in this paper). However, the use of simple, downloadable programs (9) and the composition produced by MELTS and reported in reference 11 provide a magnetite content of ~3%.

The magnetic susceptibility of SD magnetite is very complex, depending on grain size, shape, grain size distribution, and temperature (36). Grain size distributions are typically lognormal and result in an apparently linear behavior for large temperature ranges (36). Accordingly, I use a linear magnetic susceptibility based on a formula derived from data in reference 15, in which ρ_M equals 5200 $\mathrm{kg/m^3}$.

$$\chi(T) = \begin{cases} \left[1.8 \times 10^{-4} + \frac{(T-50)\left(1.2\times10^{-4}\right)}{250}\right] \times \rho_M, T < 858\ \mathrm{K} \\ 0, T > 858\ \mathrm{K} \end{cases} \text{ [SI units]} \qquad (10)$$

To determine the magnetic field produced by the permanent crustal magnetization, a 2-D vertical section of the hypothetical crust is discretized into prisms. Each prism is assigned a magnetization based on its temperature (obtained from the thermal modeling) and its assumed magnetite content. I then calculate the magnetic field

of each prism using the analytic formula presented in reference 2 and then sum the magnetic fields to obtain the magnetic anomaly at each location along a selected meridional swath as shown in Figure 4. This is performed for each of the ten selected times in the thermal evolution. The maximum radial extent in the thermal model is 4 km. This relatively short radius creates deleterious edge effects as the simulated flyby altitude becomes very high. The vertical distribution of magnetic susceptibility values calculated at the maximum radial extent is assumed to apply out to 16 km in order to reduce these edge effects.

4.4 Magnetic Results

Figure 7 shows the corresponding approximate magnetic susceptibilities of SD magnetite for the thermal distribution shown in figure 6. A corresponding "bubble" of increased magnetic susceptibility can be seen. In this model, magnetic susceptibility increases with temperature until the Curie temperature, at which the magnetic susceptibility goes to zero. The local susceptibility maximum is a result of the higher surface porosity slowing the diffusion of thermal energy.

Figure 8 shows the magnetic signal modeled for a satellite during a flyby that passes directly over the volcanic pipe at an altitude of 100 km for a 160 m pipe, crustal thickness of 30 km, and surface porosity of 0.3. The volcanic center is located at the equator with the swath directed meridionally. This produces the same magnetic anomaly as created by a volcanic center located at either pole, though the value of the anomaly switches from positive to negative. The inducing field of Jupiter is considered uniformly downward relative to the ecliptic plane. At this altitude, there is no measurable anomaly,

only a background field of approximately -33 nT. The altitude must be decreased to 1 km for an anomaly to be detected. Figure 9 shows magnetic anomaly for satellite flybys at an altitude of 1 km for similar models to those of Figure 8. The maximum value of the calculated magnetic near-field anomaly in this case increases to ~110 nT. The background magnetic field reaches a maximum strength of approximately -568 nT, causing a maximum magnetic anomaly of ~140 nT. Figure 10 shows the magnetic anomaly produced at an altitude of 1 m holding all other variables the same. The maximum amplitude of the anomaly is increased to ~1000 nT, with a maximum background field of approximately -650 nT. Figures 11 through 13 are the magnetic anomalies for a 90 km thick crust at altitudes of 100 km, 1 km, and 1 m. At a 100 km altitude, the anomaly is again undetectable, but the background field has increased to -67 nT. At 1 km, the magnetic anomaly has a strength of ~110 nT, with a background field of -760 nT. Figure 13 shows the variation of the magnetic anomaly at an altitude of 1 m for a crustal thickness of 90 km. The maximum value of the calculated magnetic anomaly is ~1000 nT with a background field of -800 nT.

5. DISCUSSION AND CONCLUSION

The 1-D thermal modeling predicts a steady-state crustal temperature that maintains the surface value to the base of the lithosphere, which is significantly deeper than that predicted byreference 17. The modeling also predicts a geotherm that is significantly less dependent on porosity due to the great depth to which the region of rapid temperature change (and hence a rapid change in thermal diffusivity) is found. The 1-D modeling in this work predicts a geotherm very similar to that of the analytical solution. This is due to the very small variation in thermal diffusivity of the lunar analogue used. Across large changes in temperature, the thermal diffusivity of lunar rock changes very little. The large changes in temperature occur near the base of the thermal lithosphere, where the pore space has been reduced to very small amounts (less than a few percent).

Reference 17 discussed the possible thermal effects of sulfur and sulfur dioxide aquifers in the lithosphere. A significant amount of solid sulfur and sulfur dioxide is advected downward with the lithosphere. At great depths, where the temperature is sufficiently high, these materials exist as a liquid and may travel through fractures in the lithosphere to act as aquifers. These aquifers provide necessary volatiles to the magma to ensure surface eruptions. Without the addition of sulfur and/or sulfur dioxide, the density of the magma would remain greater than the host rock and prevent ascent (17). The depth at which these aquifers can form is controlled, in part, by the temperature of the lithosphere. As the temperature is reduced for a large portion of the lithosphere, this would shift the aquifers deeper than previously predicted. This does not seem to modify

the conclusions of reference 17. Their work shows sulfur and sulfur dioxide reservoirs forming at depths below the maximum ascent of magma.

The 2 D thermal modeling predicts the upper 80% of the volcanic pipe will cool below 429 K within a relatively short time period (less than 7,000 years for a pipe of 160 m radius), with a warm bubble in the upper few kilometers being the last to cool beneath this temperature. This temperature is well below that required for sulfur volcanism and is approximately that required for SO_2 volcanism (17). This would suggest silicate volcanism becomes indistinguishable from other sources very quickly. Problematically, this work does not include the effects of latent heat of crystallization, a radiative surface boundary, a more realistic geometry, or continuous eruptions. The radiative surface boundary and a more realistic geometry are not addressed here, but should be included for future examinations of the crust of Io. The magma conduits of Io are expected to be dikes several tens of kilometers in extent, possibly becoming funnel-shaped (like diatremes) near the surface. This change would increase the amount of energy going into the surrounding lithosphere while reducing energy loss from the pipe. Such a geometry is expected to produce a similar thermal evolution and have little effect on the magnetic anomaly detected at satellite altitude.

The magma that freezes in the volcanic pipe will release latent heat of crystallization, so these models underestimate the heat output from the pipe. The portion of energy missing and its importance can be estimated by a simple comparison of the sensible heat per mass of cooling lava (specific heat times the temperature change) to the latent heat. ($C \times \Delta T: L$). Reference 17 report a latent heat of crystallization of $6.05 \times$

$10^5 \frac{J}{kg}$ and an average specific heat of 1336 $\frac{J}{kg\ K}$ (though plausible specific heats could be as low as 1000 $\frac{J}{kg\ K}$.) For a change in temperature of 1400 K (eruption minus background temperature), the resulting ratio is about 3 (2.4). Therefore, the latent heat represents an appreciable, but smaller, contribution of approximately 24 (4) percent of the total heat release. Qualitatively, the thermal evolution of the 2 D instantaneously emplaced pipe is unchanged. Including the latent heat would slow the cooling of the pipe and increase the temperature in the nearby lithosphere. The pipe would remain above 429 K for a significantly longer period. This would result in a slightly broader magnetic anomaly with a slightly stronger magnetization near the pipe, but would ultimately create a similar magnetic anomaly.

Io has eruptive centers that have been active for the entirety of spacecraft observation. While this is a relatively short time (~30 years), several scientists estimate eruptions may continue for hundreds and even hundreds of thousands of years based on the lateral extent of paterae (12, 21). Such a volcanic center would release a much larger amount of energy into the surrounding crust. This would considerably increase the temperature around the volcanic center and require much longer to cool below the temperature of sulfur and SO_2 volcanism. The finite radial extent of the thermal perturbations is the cause of the missing anomaly at higher altitudes. As altitude increases, short wavelength (high wavenumber) contributions are attenuated in a predictable manner. It is, essentially, a low-pass filter. This is often used to perform upward continuation of potential data to remove the effect of shallow anomalies and to compare potential data acquired at differing altitudes (2). The 160 m pipe only affects

material within ~1.5 km, a distance much smaller than the nominal altitude considered. This radial extent quickly becomes short wavelength with increasing altitude. Conversely, this means long wavelength features of the same strength are only weakly attenuated (2). The background crustal field at 100 km is -33 nT, which reduces to -0.3 nT for a 1% magnetite crust. This is nearly at the sensitivity limit of the proposed *IVO*. A sufficiently large demagnetized or thermally perturbed (as increased temperature causes increased susceptibility) radial extent may produce a detectable magnetic anomaly. A volcanic center active for hundreds, thousands, or tens of thousands of years will create significantly broader thermal perturbations. Such an extended eruption may be of sufficiently long wavelength to avoid the attenuation of the low-pass filtering of the upward continuation effect. Additionally, such a continuous eruption places a broad, thin layer of lava on the surface on the order of 10-20 meters (18). This thin layer of lava will heat the underlying rock and increase its magnetic susceptibility. This will increase the magnetic anomaly very close to the surface, such as the 1 m altitude, but has little effect at great distance as the altered and additional layer are so thin compared to the thickness of the crust.

I do not estimate the amounts of magnetite that might be present in the Io crust. However, Earth analogues typically have 1% magnetite. At satellite altitude of 1 m (an impossibly low value, but this provides the strongest signal) for a crust of 30 km thickness and surface porosity of 0.3, a value of 1% magnetite content would generate an initial magnetic anomaly of ~10 nT. This is well below the sensitivity of the proposed fluxgate magnetometer, making the magnetic anomaly impossible to detect. At the

higher altitude shown in figure 10, the 1% magnetite magnetic anomaly would be approximately ~1 nT. These are detectable, but weak and require unrealistically low flyby altitudes. Higher, more realistic, altitudes exacerbate this problem, as shown in Figure 8 with a flyby altitude of 100 km. The magnetic signal modeled is a flat response. Figure 14 shows a log/log contour of the maximum magnetic anomaly as a function of pipe radius and observation altitude. Even for what are presumed to be unrealistically large pipe radii, the magnetic anomaly is undetectable at expected flyby altitudes. Magnetic anomalies on Mars were easily detected by *Mars Global Surveyor* (*MGS*) at its nominal orbital altitude of 400 km (6). The magnetic anomalies measured by *MGS* reached values greater than 30 nT (29). Why are anomalies on Io so much smaller? The anomalously magnetized regions of Mars extend as far as 2,000 km laterally, and 100 km along strike (29). This much larger area results in a large wavenumber anomaly which is less attenuated by distance from the source. The effect of continuous eruptions is to be considered quantitatively in future work. Additionally, the modeled crust in this work obtains a maximum magnetization of 2.9 A/m, which reduces to 0.029 A/m for a 1% magnetite crust, whereas estimates for the magnetization of Mars are 20 A/m. The current inducing field of Jupiter only weakly magnetizes the crust at the orbit of Io. If a signal is detected from the crust, it 1) is most likely the result of shock magnetization due to impacts; 2) implies the Jupiter field was several orders of magnitude stronger in the recent past; 3) Io possessed a geodynamo of some sort producing a magnetosphere comparable to the Earth's; 4) or the crust is thermally perturbed by more voluminous magma bodies or continuous eruptions. Shock magnetization encounters similar

problems with short wavelengths attenuating at altitude, and there is no evidence of drastic variation in the Jupiter magnetosphere (35). The third is a distinct possibility as Io must have experienced some change to its orbital or thermal evolution (24, 28). Steady-state tidal models predict significantly lower energy output and suggest periodic heating and cooling (24, 29). A past era of cooling may have allowed a solid core and a geodynamo to form (and which was destroyed by subsequent heating) and strongly magnetize the crust (18, 27). The crust of Io is recycled at a rate of ~1 cm/yr. This requires an approximate 10 km thick layer of the crust be destroyed every 100,000 years. Though the thickness of the crust is poorly constrained, the detection of a crustal anomaly would require drastically different conditions at Io within the past one million years, and likely much more recently than that. Problematically, this requires extensive volcanism to continue despite an overall cooling of the planet.

REFERENCES

(1) B. J. Anderson, M. H. Acuña, H. Korth, J. A. Slavin, H. Uno, C. L. Johnson, M. E. Purucker, S. C. Solomon, J. M. Raines, T. H. Zurbuchen, G. Gloeckler, & R. L. McNutt Jr. (2010). "The Magnetic Field of Mercury." *Space Science Review.* Vol 152. Pg 307-339.

(2) R. J. Blakely. (1995). "Potential Theory in Gravity & Magnetic Applications." *Cambridge University Press.*

(3) R. F. Butler. (1992). "Paleomagnetism: Magnetic Domains to Geologic Terranes." *Blackwell Scientific Publications.*

(4) V. Cataldo, L. Wilson, & G. Leone. (2001). "Ascent and Eruption of Magmas on Io: Application to Pele." *Lunar and Planetary Science XXXII.*

(5) D. A. Clark. (1997). "Magnetic Petrophysics and Magnetic Petrology: Aids to Geological Interpretation of Magnetic Surveys." *Journal of Australian Geology & Geophysics.* Vol 17. Pg 83-103.

(6) J. E. P. Connerney, M. H. Acuña, N. F. Ness, G. Kletetschka, D. L. Mitchell, R. P. Lin, & H. Reme. (2005). "Tectonic Implications of Mars Crustal Magnetism." *Proceedings of the National Academy of Sciences.* Vol 102. No. 42. Pg 14970-14975.

(7) N. Fujii & M. Osako. (1973). "Thermal Diffusivity of Lunar Rocks under Atmospheric and Vacuum Conditions." *Earth and Planetary Science Letters.* Vol 18. Pg 65-71.

(8) C. W. Hamilton, C. D. Beggan, S. Still, M. Beuthe, R. M. C. Lopes, D. A. Williams, J. Radebaugh, & W. Wright. (2012). "Spatial Distribution of Volcanoes on Io: Implications for Tidal Heating and Magma Ascent." *Earth and Planetary Science Letters*. Vol. 361. Pg 272-286. http://dx.doi.org/10.1016/j.epsl.2012.10.032

(9) K. Hollocher. "norm4." [Microsoft Excel]. <http://minerva.union.edu/hollochk/c_petrology/norms.htm>. Accessed: 1 May 2014.

(10) T. V. Johnson. (1999). "Io." The New Solar System. Chapter 17, *Sky Publishing Corporation*., pages 241-252.

(11) L. Keszthelyi, W. Jaeger, M. Milazzo, J. Radebaugh, A. G. Davies, & K. L. Mitchell. (2007). "New Estimates for Io Eruption Temperatures: Implications for the Interior." *Icarus.* Vol 192. Pg 491-502.

(12) L. Keszthelyi, W. L. Jaeger, E. P. Turtle, M. Milazzo, & J. Radebaugh. (2004). "A Post-Galileo View of Io's Interior." *Icarus*. Vol 169. Pg 271-286.

(13) K. K. Khurana, X. Jia, M. G. Kivelson, F. Nimmo, G. Schubert, & C. T. Russell. (2011). "Evidence of a Global Magma Ocean in Io's Interior." *Science.* Vol 332. Pg 1186-1189.

(14) M. R. Kirchoff, W. B. McKinnon, & P. M. Schenk. (2011). "Global Distribution of Volcanic Centers and Mountains on Io: Control by Asthenospheric Heating and Implications for Mountain Formation." *Earth and Planetary Science*. Vol 301. Pg 22-30.

(15) M. G. Kivelson, K. K. Khurana, C. T. Russell, S. P. Joy, M. Volwerk, R. J. Walker, C. Zimmer, & J. A. Linker. (2001). "Magnetized or Unmagnetized: Ambiguity Persists Following Galileo's Encounter with Io in 1999 and 2000." *Journal of Geophysical Research.* Vol 106. Pg 26121-26135.

(16) B. Langlais, V. Lesur, M. Purucker, J. E. P. Connerney, & M. Mandea. (2010). "Crustal Magnetic Fields of Terrestrial Planets." *Space Science Review.* Vol 152. Pg 223-249.

(17) G. Leone, L. Wilson, & A. G. Davies. (2011). "The Geothermal Gradient of Io: Consequences for Lithosphere Structure and Volcanic Eruptive Activity." *Icarus.* Vol 211. Pg 623-635.

(18) R. M. C. Lopes & D. A. Williams. (2005). "Io After Galileo." *Reports on ProgRess in Physics*. Vol 68. Pg 303-339.

(19) A. S. McEwen, L. Keszthelyi, J. R. Spencer, G. Schubert, D. L. Matson, R. Lopes-Gautier, K. P. Klaasen, T. V. Johnson, J. W. Head, P. Geissler, S. Fagents, A. G. Davies, M. H. Carr, H. H. Breneman, & M. J. S. Belton. (1998). "High-Temperature Silicate Volcanism on Juptier's Moon Io." *Science.* Vol 281, Pg 87-90.

(20) A. S. McEwen. (2002). "Active Volcanism on Io." *Science.* Vol 297. Pg 2220-2221

(21) A. S. McEwen, L. P. Keszthelyi, R. Lopes, P. M. Schenk, & J. R. Spencer. (2004). "The Lithosphere and Surface of Io." *Cambridge University Press.* Vol. 1. Pg 307-328.

(22) A. McEwen, E. Turtle, K. Hibbard, E. Reynolds, & E. Adams. (2012). "Io Volcano Observer (IVO): Budget Travel to the Outer Solar System." *Acta Astronautica.* Vol 93. Pg 539 – 544.

(23) W. B. McKinnon, P. M. Schenk, & A. J. Dombard. (2001). "Chaos on Io: A Model for Formation of Mountain Blocks by Crustal Heating, Melting, and Tilting." *Geology*. Vol 29. Pg 103-106.

(24) W. B. Moore. (2003). "Tidal Heating and Convection in Io". *Journal of Geophysical Research*., 108(E8), 5096, doi:10.1029/2002JE001943, 2003.

(25) A. R. Muxworthy. (1999) "Low-Temperature Susceptibility and Hysteresis of Magnetite." *Earth and Planetary Science Letters.* Vol 169. Pg 51-58.

(26) T. C. O'Reilly & G. F. Davies. (1981). "Magma Transport of Heat on Io: A Mechanism Allowing a Thick Lithosphere." *Geophysical Research Letters.* Vol 8. Pg 313-316.

(27) S. J. Peale. (2003). "Tidally Induced Volcanism." *Celestial Mechanics and Dynamical Astronomy.* Vol 87. Pg 129-155.

(28) S. J. Peale & M. H.Lee. (2002). "A Primordial Origin of the Laplace Relation Among the Galilean Satellites." *Science*. Vol 298. Pg 593-597.

(29) M. Purucker & D. Clark. (2000). "Exploration Geophysics on Mars: Lessons from Magnetics." *Leading Edge*. Vol 19(5). Pg 484-487.

(30) L. Ray, H. J. Forster, F.R. Schilling, & A. Forster. (2006). "Thermal Diffusivity of Felsic to Mafic Granulites at Elevated Temperatures." *Earth and Planetary Science Letters*. Vol 251. Pg 241-253.

(31) P.M. Schenk, R. R. Wilson, & A. G. Davies. (2004). “Shield Volcano Topography and the Rheology of Lava Flows on Io.” *Icarus*. Vol 169. Pg 98-110.

(32) A. P. Showman & R. Malhotra. (1999). “The Galilean Satellites.” *Science*. Vol 286. Pg 77-84.

(33) D. A. Williams, L. P. Keszthelyi, D. A. Crown, J. A. Yff, W. L. Jaeger, P. M. Schenk, P. E. Geissler, & T. L. Becker. (2011). “Volcanism on Io: New Insights from Global Geologic Mapping.” *Icarus.* Vol 214. Pg 91-112.

(34) D. A. Williams, A. H. Wilson, & R. Greeley. (2000). “A Komatiite Analog to Potential Ultramafic Materials on Io.” *Jounral of Geophysical Research*. Vol 105. Pg 1671-1684.

(35) Z. J. Yu, H. K. Leinweber, & C. T. Russell. (2009). “Galileo Constraints on the Secular Variation of the Jovian Magnetic Field.” *Journal of Geophysical Research.* Vol 115. doi:10.1029/2009JE003492

(36) X. Y. Zhao & Q. S. Liu. (2010). “Effects of the Grain Size Distribution on the Temperature-Dependent Magnetic Susceptibility of Magnetite Nanoparticles.” *Science China Earth Sciences*. Vol 53. Pg. 1071–1078. doi:10.1007/s11430-010-4015-y

(37) K. Boggs & S. Lavoie. “PIA00208: Global Image of Io (True Color).” <http://photojournal.jpl.nasa.gov/> Accessed: 10 December 2014.

APPENDIX A

FIGURES

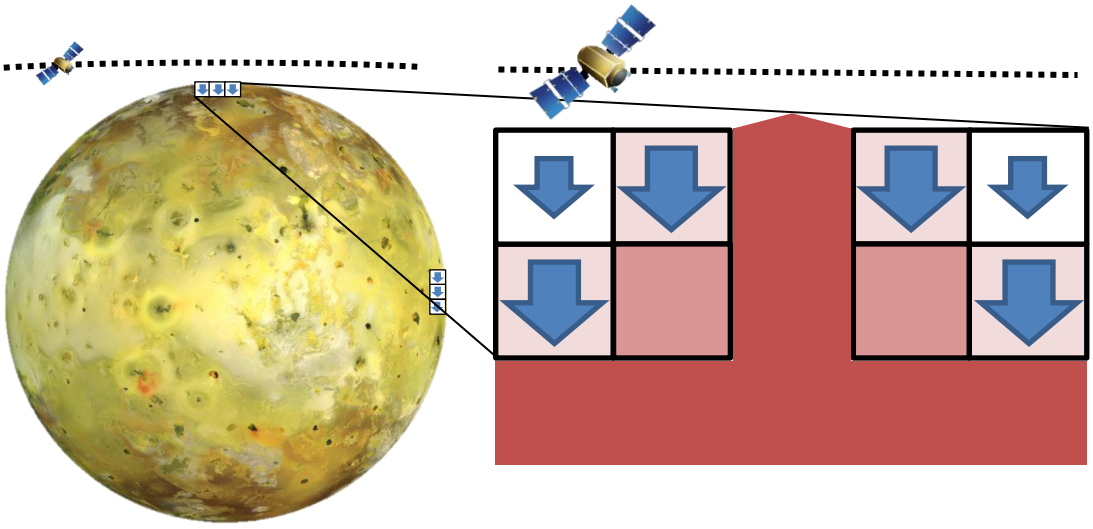

Figure 1. Conceptual depiction of the satellite flyby and the magnetization around a volcanic center. Arrows depict the direction and strength of the magnetization adjacent to a volcanic pipe. The magnetic susceptibility (and hence magnetization) increase with temperature until the Curie temperature is reached, at which point the magnetization goes to zero. Image of Io courtesy of NASA/JPL (37).

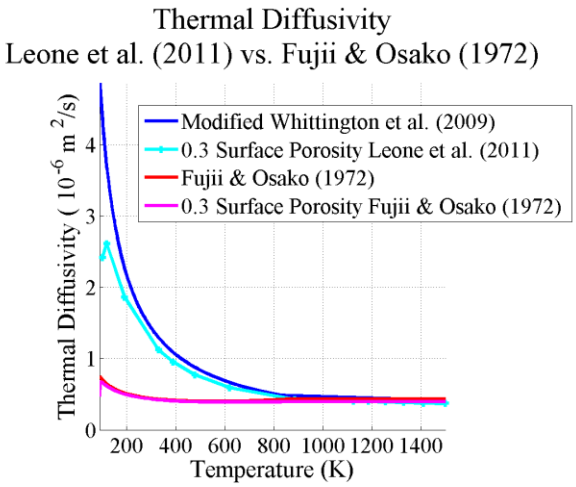

Figure 2. Thermal diffusivity versus temperature. This is a plot of thermal diffusivity of the modified Whittington et al. (2009) equation, reported values of thermal diffusivity with an initial surface porosity of 30% from Leone et al. (2011), the thermal diffusivity of the Fujii & Osako (1972) equation for a lunar rock with 5.5% porosity, and thermal diffusivity with an initial surface porosity of 30% for the same lunar rock. At high temperatures, all four are approximately the same value, but diverge at low temperatures.

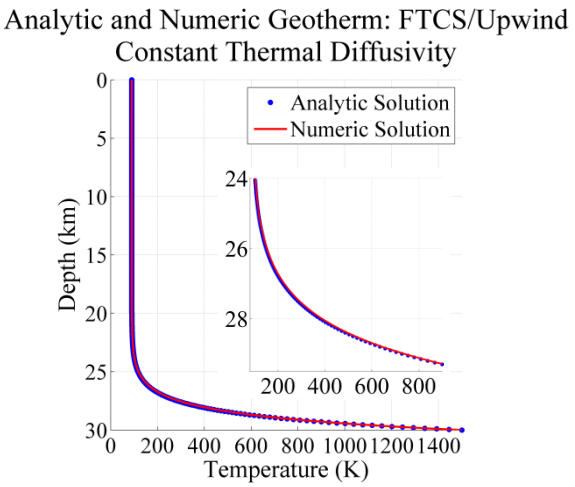

Figure 3. Analytical versus numerical solution of the geotherm for constant thermal diffusivity. This shows the difference between the analytical solution of O'Reilly and Davies (1981) versus my numerical solution. In this, the analytic and numeric solution use a constant diffusivity of 4×10^{-7} m^2/s. This provides a simple assessment of the numerical solutions accuracy.

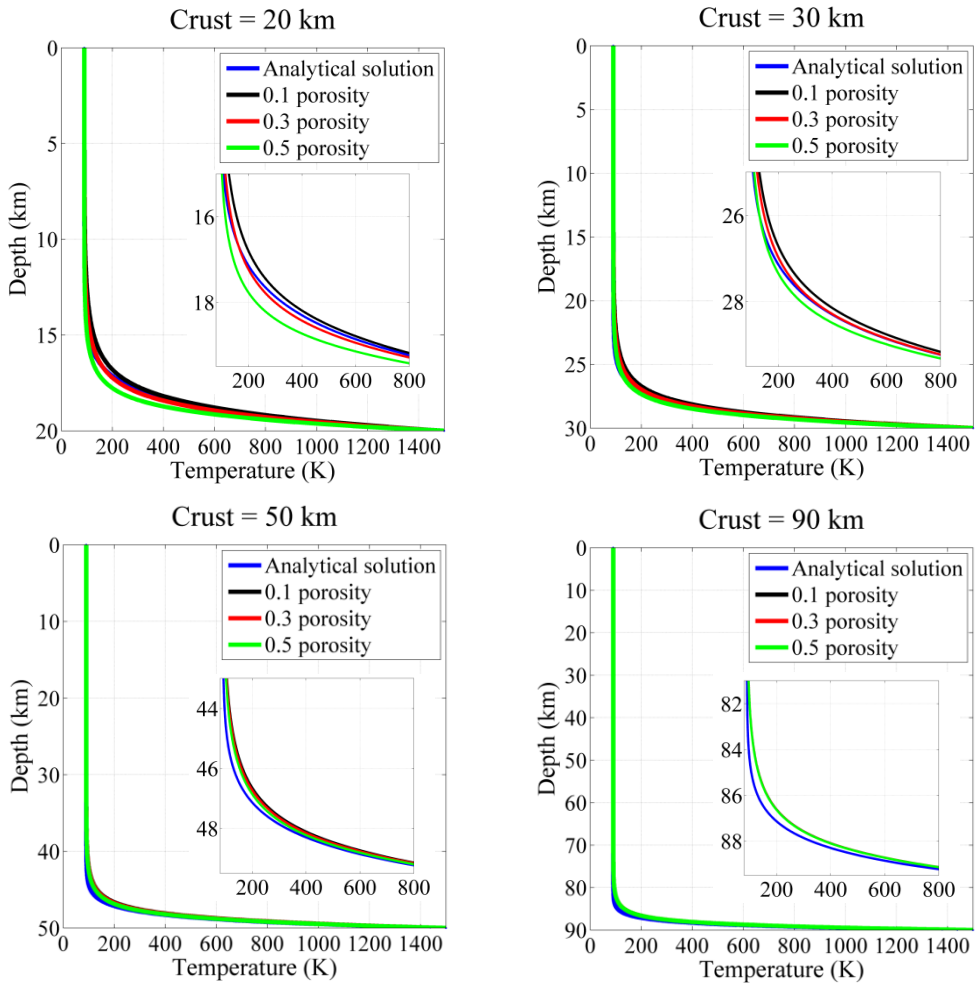

Figure 4. Analytical versus numerical solution for variable diffusivity and multiple surface porosities. Depicted are the analytical solution and numerical solutions for the 1 D geotherm for surface porosities of 0.1, 0.3, and 0.5, and for crustal thicknesses of 20, 30, 50, and 90 kilometers. Insets are included of intermediate depths, at which the rate of change and difference between the analytical and numerical solutions are greatest. The analytical solution uses a thermal diffusivity of $4 \times 10^{-7} \mathrm{m}^2/\mathrm{s}$, and the numerical solutions use the thermal diffusivity in equation 5 as modified by porosity.

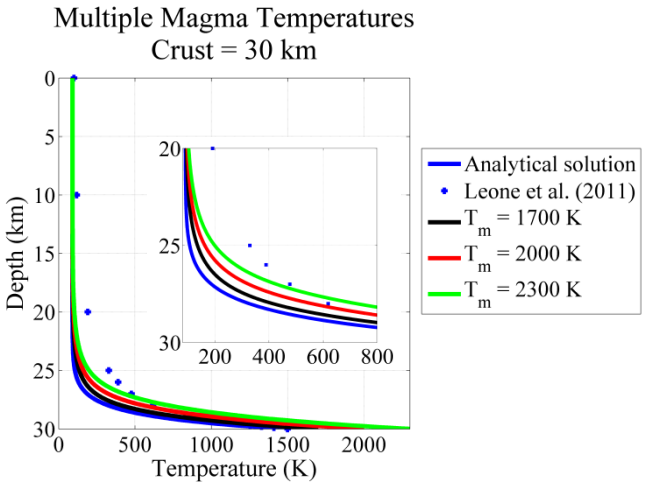

Figure 5. Geotherm for multiple mantle temperatures. The analytical solution and Leone et al. (2011) geotherm versus my numerical solution for different temperatures of the thermal lithosphere boundary. This is for a 30 km lithosphere with an surface porosity of 0.3. At intermediate depths, the lithosphere has a cooler temperature than that predicted by Leone et al. (2011) despite the much higher thermal lithosphere boundary temperature.

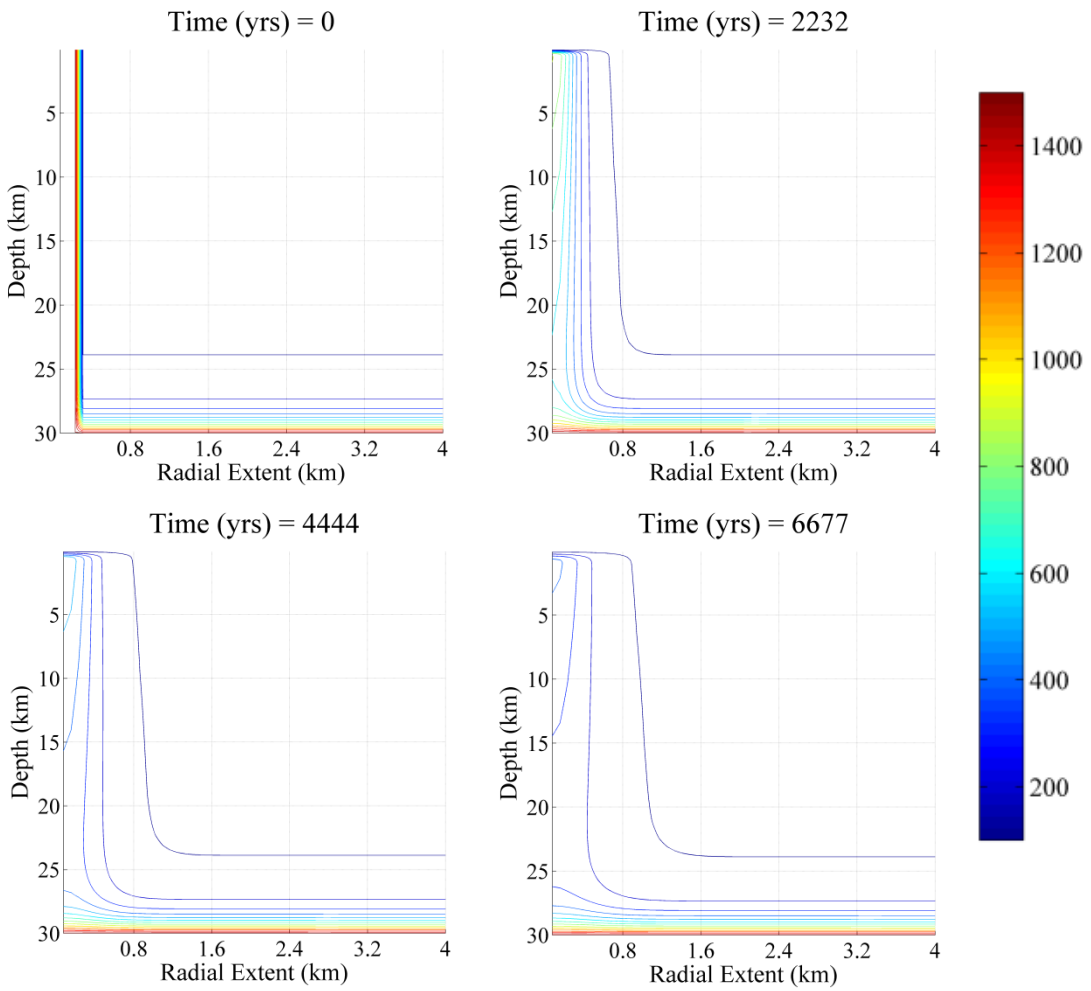

Figure 6. 2 D Thermal thermal Evolutionevolution of the thermal lithosphere. Displayed is the 2 D thermal evolution for crustal thickness of 30 km, surface porosity of 0.5, and pipe radius of 160 m. The temperature scale is in kelvin. Contours are spaced every 100 K. A warm "bubble" is created near the top of the volcanic pipe due to the reduced thermal diffusivity caused by increased porosity near the surface. The times depicted correspond to initial emplacement (zero years), 2232 years after emplacement, 4444 years after emplacement, and 6677 years after emplacement.

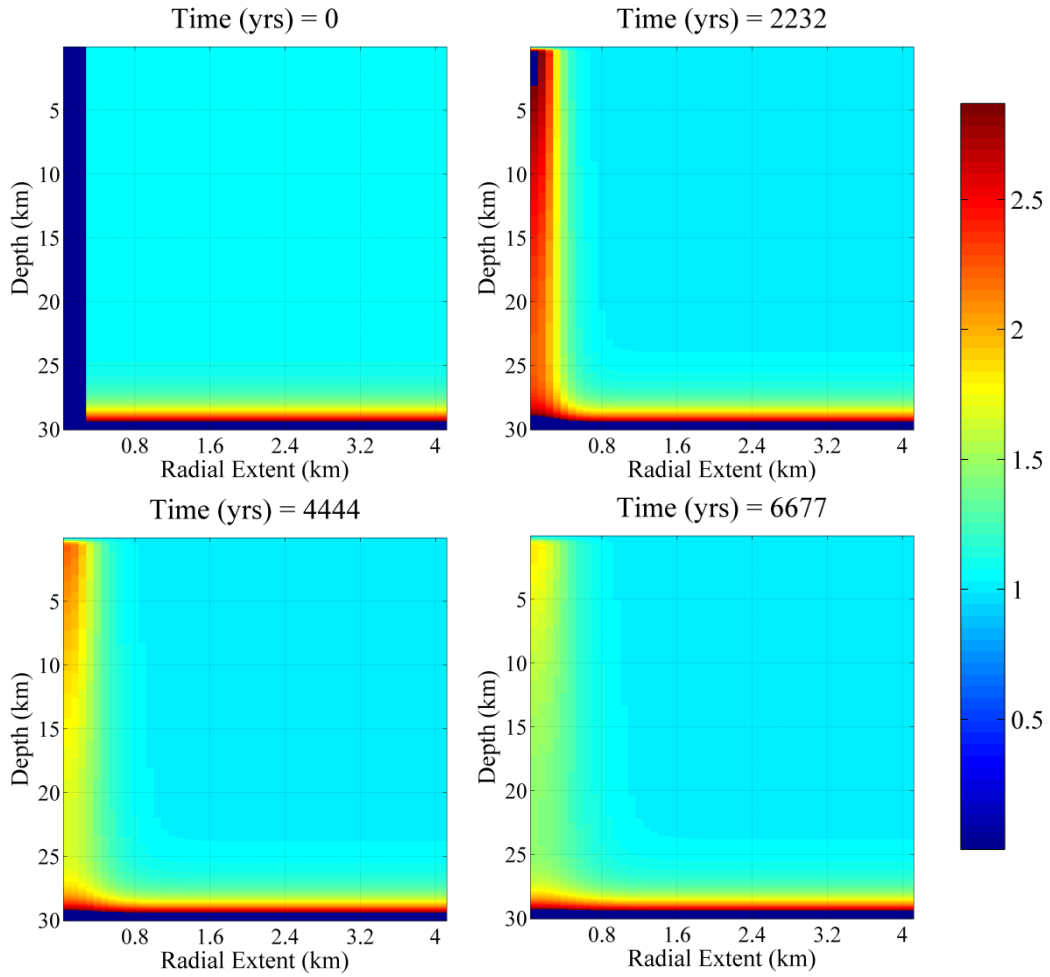

Figure 7. 2 D Magnetic susceptibility evolution. These depict the magnetic susceptibilities of magnetite for the temperatures shown in Figure 5. The susceptibility is in SI units. A "bubble" of high magnetic susceptibility (surrounding a core of zero susceptibility at 2232 years) reflects the increased temperature in these regions.

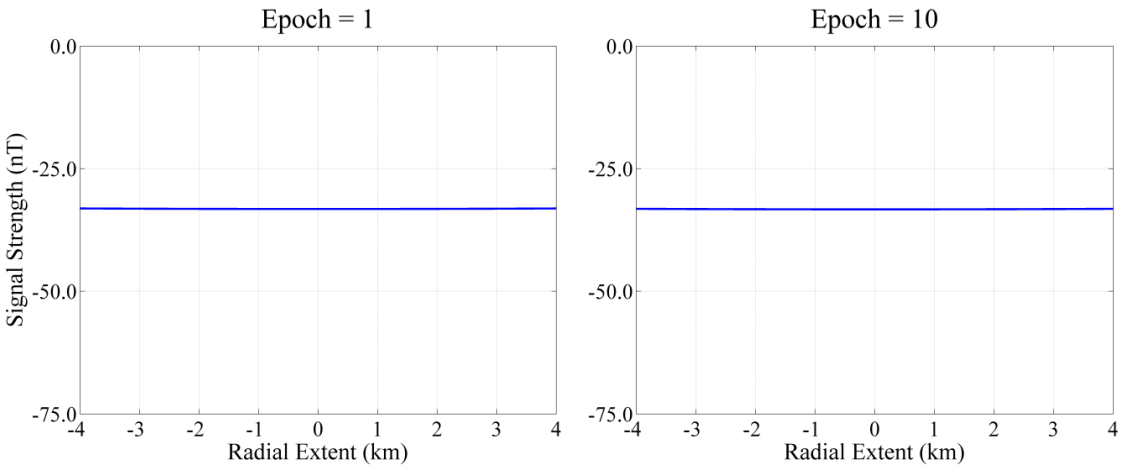

Figure 8. Magnetic anomaly produced by a volcanic pipe of radius 160 m, porosity 0.3, and crustal thickness of 30 km at an altitude of 100 km. Epoch 1 corresponds to the initial emplacement, and Epoch 10 corresponds to the end of the modeling. At this altitude, there is no magnetic anomaly, only a background field from the crust of -33 nT.

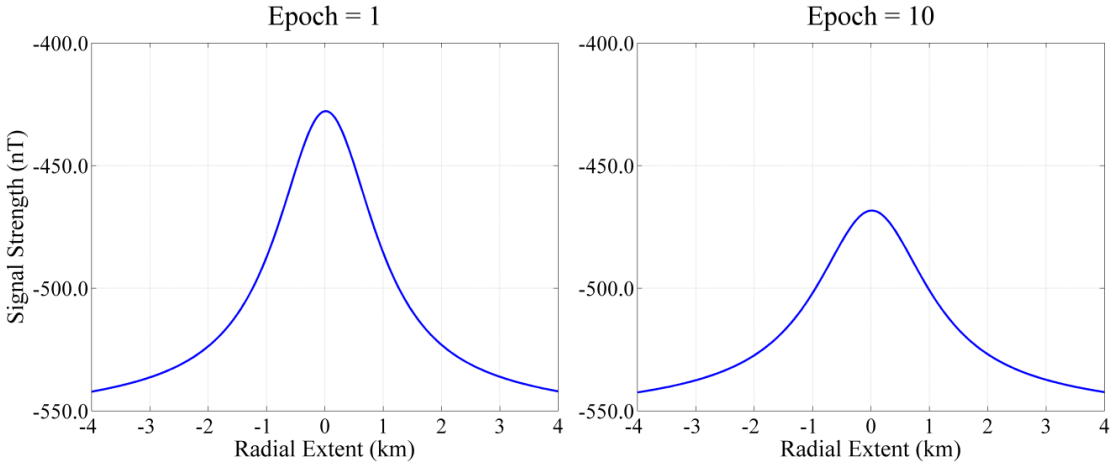

Figure 9. Magnetic anomaly produced by a volcanic pipe of radius 160 m, porosity 0.3, and crustal thickness of 30 km at an altitude of 1 km. The magnetic anomaly reaches an apparent maximum of ~110 nT in a background field of approximately -540 nT. The maximum strength of the background field reaches approximately -568 nT.

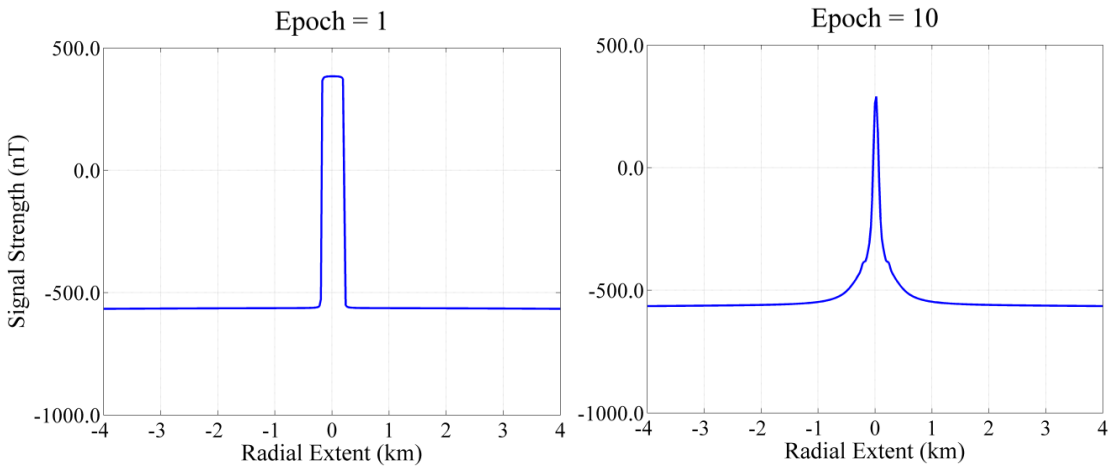

Figure 10. Magnetic anomaly produced by a volcanic pipe of radius 160 m, porosity 0.3, and crustal thickness of 30 km at an altitude of 1 m. Epoch 1 corresponds to the initial emplacement, and Epoch 10 corresponds to the end of the modeling. This crust modeled at an impossibly low altitude produces a maximum magnetic anomaly of approximately 1000 nT in a background field of approximately -650 nT.

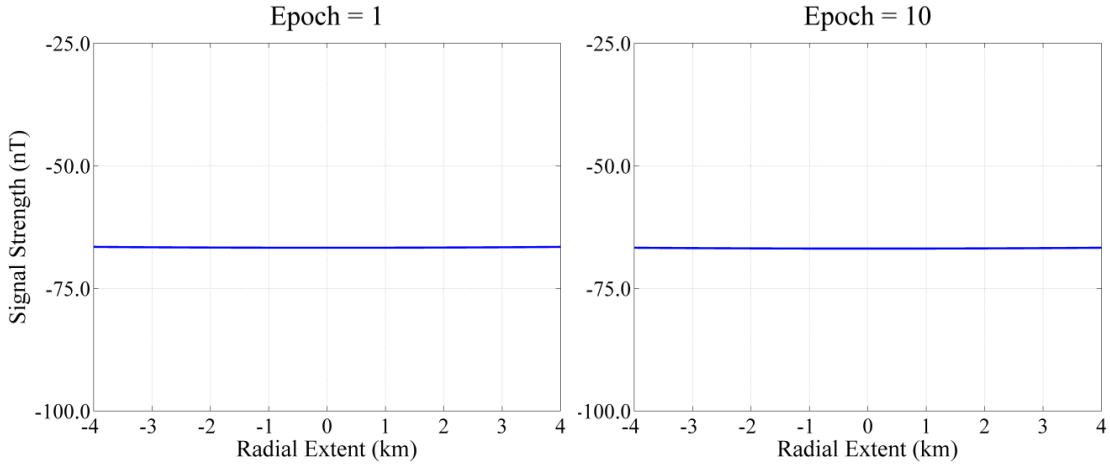

Figure 11. Magnetic anomaly produced by a volcanic pipe of radius 160 m, porosity 0.3, and crustal thickness of 90 km at an altitude of100 km. At this altitude, there is no magnetic anomaly, only a background field from the crust of -67 nT.

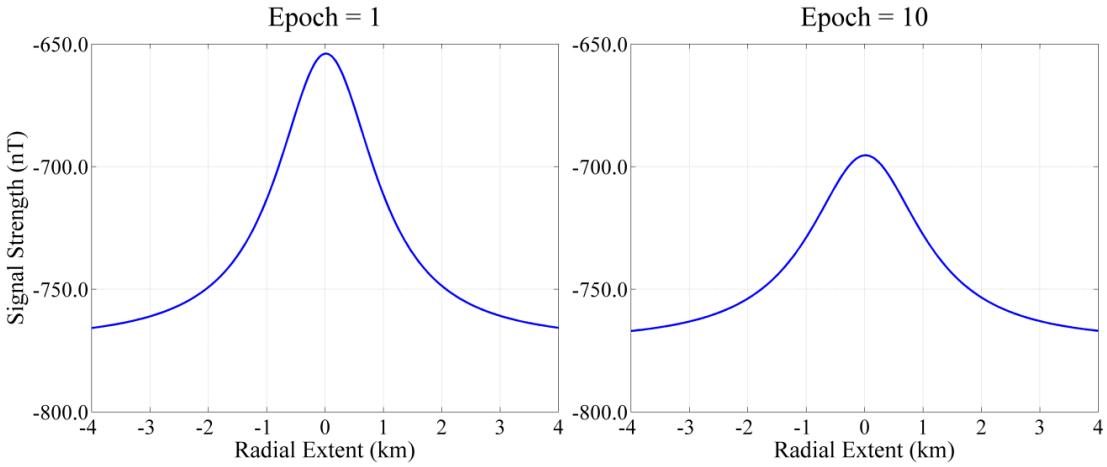

Figure 12. Magnetic anomaly produced by a volcanic pipe of radius 160 m, porosity 0.3, and crustal thickness of 90 km at an altitude of1 km. At this altitude, there magnetic anomaly reaches a value of ~110 nT, with a background field from the crust of -760 nT.

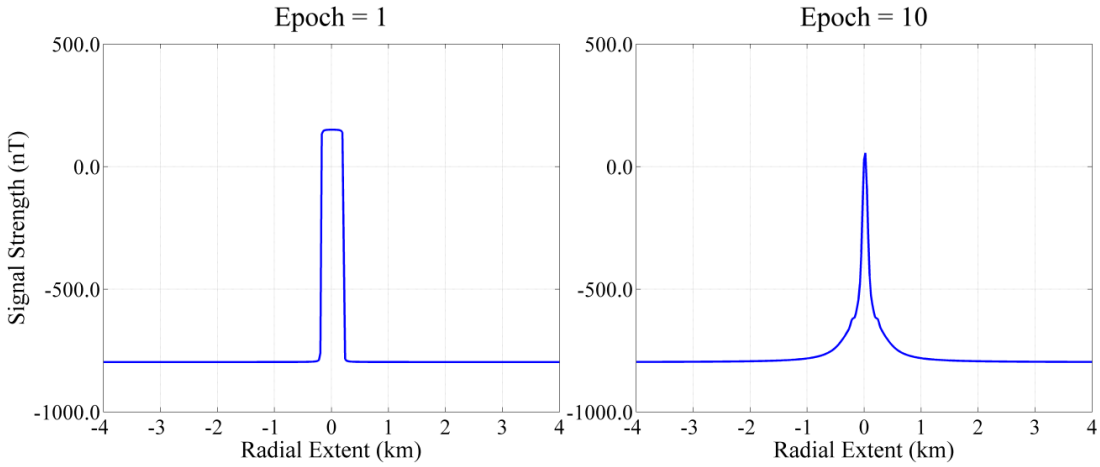

Figure 13. Magnetic anomaly produced by a volcanic pipe of radius 160 m, porosity 0.3, and crustal thickness of 90 km at an altitude of1 m. At this altitude, there magnetic anomaly reaches a value of ~1000 nT, with a background field from the crust of -800 nT.

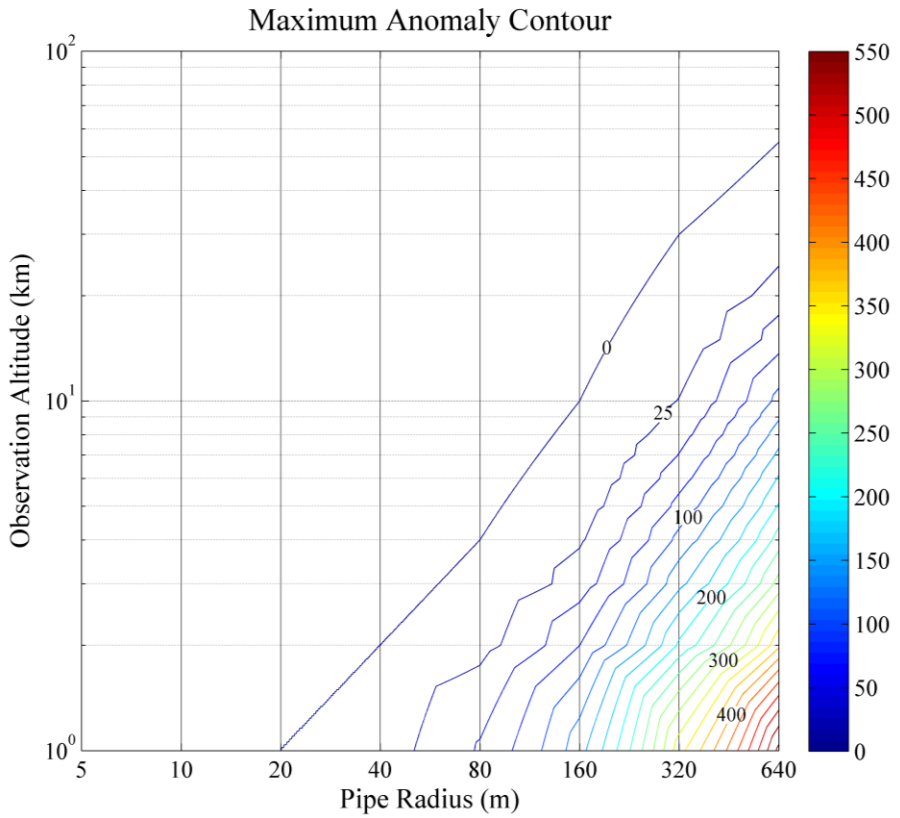

Figure 14. Log/log contour of the maximum magnetic anomaly as a function of pipe radius and observation altitude. These values are modeled from the initial emplacement for a 100% magnetite lithosphere. Contours are in units of 25 nT. The largest modeled pipe, 640 m in radius, is detectable by the proposed *IVO* (minimum of 0.25 nT anomaly) at an altitude of ~25 km or lower.